AIP Journal of Applied Physics

Nanotwins and phases in high-strain Pb (Mg 1 / 3 Nb 2 / 3) 1 − x Ti x O 3 crystal

C.-S. Tu, C.-M. Hsieh, R. R. Chien, V. H. Schmidt, F.-T. Wang, and W. S. Chang

Citation: Journal of Applied Physics **103**, 074117 (2008); doi: 10.1063/1.2904900
View online: http://dx.doi.org/10.1063/1.2904900
View Table of Contents: http://scitation.aip.org/content/aip/journal/jap/103/7?ver=pdfcov
Published by the AIP Publishing

Nanotwins and phases in high-strain $Pb(Mg_{1/3}Nb_{2/3})_{1-x}Ti_xO_3$ crystal

C.-S. Tu,[1,a)] C.-M. Hsieh,[1] R. R. Chien,[2] V. H. Schmidt,[2] F.-T. Wang,[1] and W. S. Chang[3]
[1]*Department of Physics, Fu Jen Catholic University, Taipei 242, Taiwan*
[2]*Department of Physics, Montana State University, Bozeman, Montana 59717, USA*
[3]*Department of Mechanical Engineering, National University of Singapore, Singapore 112960, Singapore*

(Received 24 January 2008; accepted 5 February 2008; published online 14 April 2008)

This work is a study of the thermal stability of (001)-cut $Pb(Mg_{1/3}Nb_{2/3})_{1-x}Ti_xO_3$ ($x=0.30$) single crystals before and after an electric (E)-field poling by means of dielectric permittivity, hysteresis loop, domain structure, polarization current, and x-ray diffraction. An $R(R_{NT})$-$R(R_{NT})$/$T(T_{NT})$-$T(T_{NT})$-C transition sequence was observed upon heating in the unpoled sample. R, R_{NT}, T, T_{NT}, and C are the rhombohedral, rhombohedral nanotwin, tetragonal, tetragonal nanotwin, and cubic phases, respectively. R/T indicates coexistence of the R and T phases. $R(R_{NT})$ and $T(T_{NT})$ indicate that the R_{NT} and T_{NT} structures mimic monoclinic phases in the R and T matrices, respectively. After a prior E-field poling, an $R(R_{NT})$-$T(T_{NT})$-C phase sequence takes place upon heating. The dielectric permittivity and current density evidenced an additional polarization at 355 K, which is associated with the vanishing of the dielectric dispersion, which reappears near 410 K and remains up to the Burns temperature $T_B=510$ K. This study suggests that nanotwins (R_{NT} and T_{NT}) can play an important role in high-strain piezoelectric crystals while phase transition takes place. Under $E=38$ kV/cm, [001] T domains randomly appeared in the matrix, suggesting that the matrix consists of a glassy matrix and ferroelectric nanoclusters. © *2008 American Institute of Physics*. [DOI: 10.1063/1.2904900]

I. INTRODUCTION

An important feature of relaxor ferroelectrics is the existence of polar nanoclusters [or polar nanoregions (PNRs)], which are believed to be responsible for ferroelectric (FE) properties and giant piezoelectricity. Field-cooled and zero-field-cooled ^{207}Pb nuclear-magnetic-resonance (NMR) spectra of the $Pb(Mg_{1/3}Nb_{2/3})O_3$ (PMN) prototype relaxor crystal showed the existence of two components—an isotropic spherical glass matrix and an anisotropic FE nanoclusters.[1,2] Also, Pb nuclei are displaced in the spherical glass matrix at 290 K ($>T_C\cong 210$ K), but there is no preferential frozen orientation or magnitude of displacement.[2] The FE polar clusters, which can respond to an external E field (greater than the threshold field E_t), are embedded in the single-dipole-glass matrix, which does not appreciably respond to an E field.[2] About 50% of the Pb nuclei reside in the spherical glass matrix and 50% in the FE polar nanoclusters.[2] An extra peak was observed near 210 K in the field-heated/field-cooled dielectric spectra, implying a first-order FE transition.[3] A neutron analysis of unpoled PMN powder shows that the volume fraction of PNRs and their correlation lengths drastically increase below 200 K.[4] Two different atomic displacements ($\delta_{c.m}$ and δ_{shift}) were proposed that are below the Burns temperature of a PMN crystal by neutron diffuse scattering.[5] $\delta_{c.m}$ is caused by soft-mode condensation and δ_{shift} represents a uniform displacement of PNRs along their polar direction, which is relative to the surrounding cubic matrix (or glassy matrix). These phenomena indicate that PMN is an incipient FE. Recent first-principles dynamic simulations for $Pb(Sc_{1/2}Nb_{1/2})O_3$ and PMN show the formation of nanoclusters in the quenched short-range-ordered regions below the Burns temperature.[6] By dielectric and domain studies, an incipient FE nature was found in $Pb(Mg_{1/3}Nb_{2/3})_{1-x}Ti_xO_3$ (PMN-xPT) crystals ($x=24\%-38\%$), in which a "hidden" transition (which was seen in unpoled samples but not as clearly as in the poled sample) was enhanced by an E field.[7] This hidden transition is associated with the appearance of monoclinic microdomains.[7]

High-strain PMN-PT and $Pb(Zn_{1/3}Nb_{2/3})_{1-x}Ti_xO_3$ crystals have demonstrated their value in piezoelectric devices,[8] and their physical properties are sensitive to the Ti content, E field, crystallographic orientation, thermal treatment, and other factors.[7,9–11] The ultrahigh piezoelectric response has been theoretically attributed to polarization rotations between the tetragonal (T) and rhombohedral (R) phases through monoclinic (M_A, M_B, and M_C) or orthorhombic (O) phases.[12] A C-T-M_C-M_A phase sequence was proposed for the field-cooled process under $E=1.0$ kV/cm in the (001)-cut PMN-30%PT crystal.[13] An R-M-T-C sequence was proposed to exist in the (001) poled PMN-30%PT crystal upon heating after the crystal was poled from the dielectric maximum temperature with $E=10$ kV/cm.[14] Polarizing microscopy revealed an M_C phase (space group Pm) in the domain structure of a (001)-cut PMN-33%PT crystal.[15] From synchrotron x-ray diffraction (XRD), an M_A phase (space group Cm) was observed in a (001) poled PMN-35%PT crystal, but the weakly poled sample exhibits an average R phase.[16]

High energy XRD results of $Pb(Zn_{1/3}Nb_{2/3})_{1-x}$-$Ti_xO_3$ ($x=0$, 4.5, and 8.0) crystals show that distinct outer layers ($\sim 10-50$ μm) are present in all of the samples.[17] An R phase was found to develop in both the outer layer and the

[a)]Author to whom correspondence should be addressed. Electronic mail: 039611@mail.fju.edu.tw.

crystal interior with increasing Ti content.[17] The polarization of FE nanoclusters and boundary conditions near the surface are believed to play an essential role in the surface distortion.[17] In PZN crystals, an *X* phase and an *R* phase were suggested for the inside crystal (bulk) and the outer layer, respectively.[18] The *X* phase has a nearly cubic lattice with a slight tetragonal distortion.[18] Similar phenomena between the outer layer and bulk have been reported in PMN-PT crystals.[19,20] High-resolution neutron scattering results show that PMN-10%PT and PMN-20%PT transform to the *X* phase below T_C.[19] The *R* distortion is limited to the outer layer. However, in PMN-27%PT, the low-temperature phase was found to be *R* in both the outer layer and the bulk. Neutron diffraction of PMN crystals reveals a strong lattice distortion and depth dependence in the surface region over a length scale of $\sim 100\ \mu$m.[21] These results indicate that the ground state inside the bulk of PMN-PT crystals prefers the *X* phase for a small Ti content and transfers to the *R* phase as the Ti content increases. On the other hand, the *R* phase has been observed in PMN-PT even for a very small Ti content by conventional XRD, which apparently probes the outer layer.[22]

A nanotwin diffraction theory that was recently developed by Wang[23,24] shows that tetragonal nanotwins of the {101} twin plane can mimic the M_C phase and rhombohedral nanotwins of the {001} and {110} twin planes can mimic the monoclinic M_A and M_B phases, respectively. Ferroelastic crystals usually consist of structural twins, accommodating the spontaneous lattice distortion and minimizing the elastic strain energy. Since the nanodomain size is much smaller than the coherent length of diffraction radiation, scattered waves from individual nanodomains coherently superimpose during diffraction, and thus, significant broadening of the reflection peak is expected.[24] In experiments, the M_A and M_B phases are always observed to be associated with the *R* phase, while the M_C phase is always observed to be associated with the *T* phase. *T*-phase nanotwins with a domain size of about 10 nm have been observed by transmission electron microscopy in PMN-PT,[25] which appear to have the M_C phase in low-resolution diffraction and polarized light microscopy.

For piezoelectric performance, an *E*-field poling is usually employed before application. However, how *E*-field poling affects the FE polarization, thermal stability, and nanostructure of the relaxor FE crystals is still not fully understood, especially for the compounds near the morphotropic phase boundary. Both in this crystal and in other (001)-cut relaxor FE crystals containing other *B*-site elements, the dielectric permittivity upon zero-field heating after a prior poling at room temperature often shows a dramatic drop (as seen in Fig. 1 at 355 K), which is followed by a large steep rise and re-entry of dielectric dispersion. No one had explained this dramatic dip before because of the following paradox: The dip appears to be similar to that seen for (001)-cut crystals of higher Ti content for which polarizing microscopy indicated a *T* structure. However, in this crystal, the polarizing microscopy showed very little *T* phase but, instead, showed an apparent *M* phase, which would give a quite stronger dielectric response for measuring the field

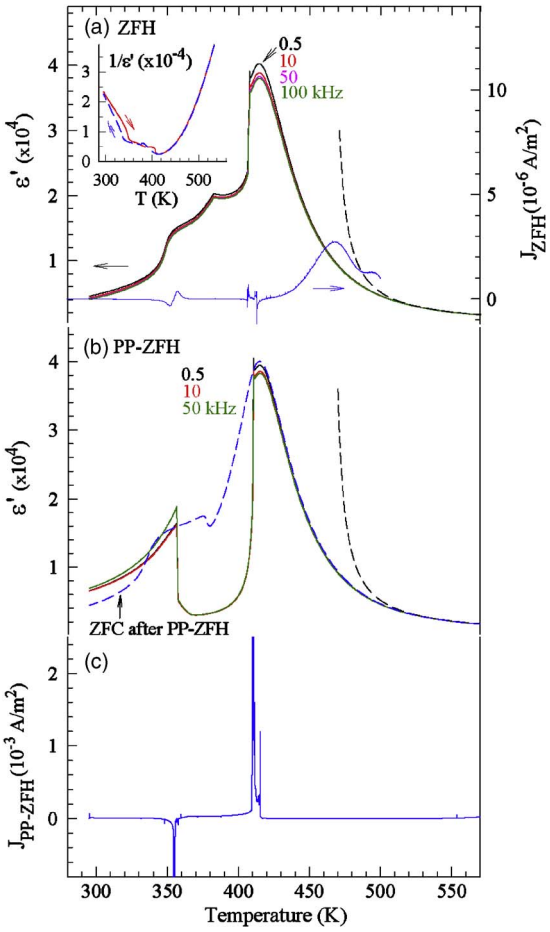

FIG. 1. (Color online) (a) ZFH dielectric permittivity and polarization current density J_{ZFH}, (b) PP-ZFH dielectric permittivity, and (c) PP-ZFH polarization current density $J_{\mathrm{PP\text{-}ZFH}}$. The $1/\varepsilon'$ and $\varepsilon'_{\mathrm{ZFC}}$ after PP-ZFH were taken at $f=10$ kHz.

along (001). In this report, we propose the *R*- and *T*-phase nanotwins to reconcile the apparently contradictory results that were seen in relaxor FE crystals of several different compositions. The existence of nanotwins can be easily mistaken as monoclinic phases (M_A, M_B, M_C) due to the averaging effect in both polarizing microscopy and x-ray diffraction.

II. EXPERIMENTAL PROCEDURE

The PMN-*x*PT (with $x=0.30$) crystal was grown by using a modified Bridgman method. A Wayne–Kerr analyzer PMA3260A was used to obtain the real part ε' of the dielectric permittivity. A sample with dimensions of $5\times5\times1$ mm^3 was cut perpendicular to the ⟨001⟩ direction, and its basal surfaces were coated with gold electrodes. Three processes were used in the dielectric studies. The first two are called "zero-field heated" (ZFH) and "zero-field cooled" (ZFC) processes, in which the data were taken upon heating and cooling without any poling. In "prior-poled zero-field heated" (PP-ZFH) process, the sample was poled at room temperature with a dc *E* field of 5 kV/cm along [001]; then, ZFH was performed without an *E* field. An irregular piezoelectric resonance was observed for $f \geq 100$ kHz in the PP-ZFH dielectric spectra. The ZFH and PP-ZFH polarization

current densities after poling at $E=5$ kV/cm were measured by using a Keithley 6517A electrometer. Hysteresis loops were taken by using a Sawyer–Tower circuit at $f=46$ Hz. A Janis CCS-450 cold head was used with a Lakeshore 340 controller for the above temperature-dependent measurements.

Domain structures were observed by using a Nikon E600POL polarizing microscope with a crossed polarizer/analyzer (P/A) pair. Transparent conductive films of indium tin oxide (ITO) were deposited on the (001) basal surfaces. The crystal thickness was about 70 μm. The angles of the P/A pair were measured with regard to the [110] direction. The experimental setup and details for using optical extinction to determine domain phases can be found in Ref. 10.

A high-temperature Rigaku model MultiFlex x-ray diffractometer with Cu $K\alpha_1$ ($\lambda=0.154\ 06$ nm) and Cu $K\alpha_2$ ($\lambda=0.154\ 44$ nm) radiations was used for the structural study of the unit cell. The intensity ratio between $K\alpha_1$ and $K\alpha_2$ is about 2:1.[26] To avoid surface stress caused by polishing, thin gold films (thickness $\cong 30$ nm) were deposited on the basal surfaces and were kept on the sample after poling. The sample thickness is 0.75 mm and the x-ray penetration depth is less than 10 μm.[17] The XRD spectra were fitted by using the PEAKFIT software with the sum of the Gaussian and Lorentzian equations. According to previous synchrotron XRD results,[19,20] both the outer layer and the inner part of the PMN-xPT crystals ($x \geq 27\%$) have the same structure. Therefore, the XRD spectra in this work can present the bulk structure.

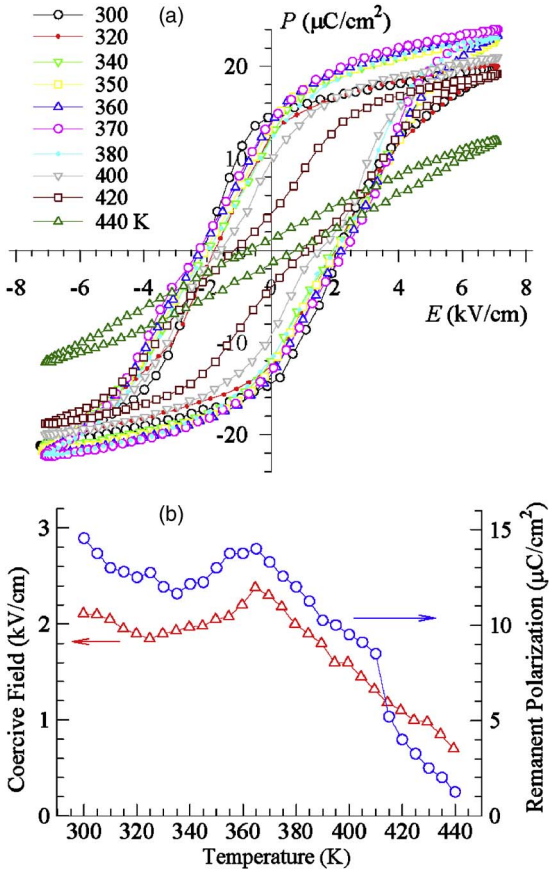

FIG. 2. (Color online) Temperature-dependent (a) hysteresis loop and (b) remanent polarization (P_r) and coercive field (E_C) upon heating.

III. RESULTS AND DISCUSSION

Figure 1 shows the [Fig. 1(a)] ZFH dielectric permittivity and polarization current density J_{ZFH}, [Fig. 1(b)] PP-ZFH dielectric permittivity, and [Fig. 1(c)] PP-ZFH polarization current density $J_{\mathrm{PP\text{-}ZFH}}$ after a prior poling at $E=5$ kV/cm. The dielectric maxima (associated with frequency dispersion) and the corresponding temperatures ($T_m \cong 415$ K) are nearly the same for ZFH and PP-ZFH. The ZFH dielectric permittivity $\varepsilon'_{\mathrm{ZFH}}$ exhibits two continuous step-up-like anomalies near 350 and 380 K. The ZFH current density J_{ZFH} shows two clear responses in the regions of 350–360 and 405–415 K, which is consistent with the two thermal hystereses in the regions of 280–360 and 380–410 K, respectively, as shown in the inset of Fig. 1(a), indicating two first-order transformations. Note from the scale at right that these currents indicate very small polarizations (downward spikes) and depolarizations (upward spikes). The ZFH polarization current J_{ZFH} is mainly associated with spontaneous polarization P_S, i.e., $J_{\mathrm{ZFH}}=-\partial P_S/\partial t$.

The PP-ZFH dielectric permittivity $\varepsilon'_{\mathrm{PP\text{-}ZFH}}$ exhibits a dramatic step-down near 355 K. The minimum E field to induce this step-down anomaly is about 1 kV/cm, which is smaller than the coercive field ($\cong 2.2$ kV/cm) at room temperature, as shown in Fig. 2. The polarization current density $J_{\mathrm{PP\text{-}ZFH}}$ shows an obvious negative response near 355 K, as seen in Fig. 1(c), which is followed by a positive peak near 410 K. These two discontinuous current responses indicate two first-order transitions near 355 and 410 K and are consistent with the thermal hystereses seen in Fig. 1(a). The PP-ZFH polarization current $J_{\mathrm{PP\text{-}ZFH}}$ is mainly associated with E-field-induced polarization P_{ind}, i.e., $J_{\mathrm{PP\text{-}ZFH}}=-\partial P_{\mathrm{ind}}/\partial t$. This pyroelectric effect is the inverse of the polarocaloric or electrocaloric effect, which was investigated in PZN-8%PT crystals by Priya and Uchino.[27] They found two negative peaks in the 315–345 K temperature range, which are followed by a positive peak near 435 K. The sign indicates whether the discontinuous change is stable or unstable. They attributed the negative peaks to a first-order R-O-T sequence because the O phase is metastable with respect to the R and T phases.[27]

How can these phenomena be explained? We start with a broad-brush explanation and fill in details as we discuss more experimental results. The prior poling develops some degree of FE order, which is probably the R phase that has polarization rotation under a [001] measuring field, and so has a relatively high permittivity compared to $\varepsilon'_{\mathrm{ZFH}}$. This order enhances the degree to which a different type of order, perhaps the T phase, can suddenly arise at 355 K. The increase in polarization at 355 K could result from this ordered phase arising at the expense of previously disordered material. At and above 355 K, these T domains have little tendency to rotate in the weak [001] measuring field and, thus, have much lower permittivity, as observed.

As the temperature increases above 355 K, as seen in Fig. 1(b), the dielectric dispersion vanishes and then completely reappears near $T_{\mathrm{re}}=410$ K, which is associated with

a multiple-peak response in $J_{PP\text{-}ZFH}$. Multiple jumps of polarization current can be interpreted as discrete changes in the size or rotation of FE microdomains or nanodomains. Here, we define T_{re} as the temperature above which the dielectric relaxation re-establishes in the crystal. Our $\varepsilon'_{PP\text{-}ZFH}$ and polarization current response are different from the result for the (001) poled PMN-30%PT crystal reported in Ref. 14, which shows three dielectric peaks and three current responses upon heating.

Both ε'_{ZFH} and $\varepsilon'_{PP\text{-}ZFH}$ were found to follow the Curie–Weiss equation, $\varepsilon' = C/(T\text{-}T_o)$, above 510 K, below which there is a noticeable deviation from the Curie–Weiss law. The dashed lines in Fig. 1 are fittings with $C = 1.8 \times 10^5$ and $T_o = 465$ K for both ε'_{ZFH} and $\varepsilon'_{PP\text{-}ZFH}$. We consider 510 K to be the Burns temperature (T_B), below which dipole glass attenuated dielectric response and polar nanoclusters begin to develop.[5] The weaker dipole glass dielectric response causes deviation from the Curie–Weiss law and the polar nanocluster dynamics are responsible for the dielectric dispersion.[28] As given in Fig. 1(b), the ZFC dielectric permittivity measured after a prior poling at $E = 5.0$ kV/cm shows a similar behavior as seen in ε'_{ZFC} above T_{re} and has the same Burns temperature. This indicates that the polarized state induced by an E field can be erased by thermal annealing.

Figure 2(a) shows the temperature-dependent hysteresis loops and Fig. 2(b) shows the remanent polarization (P_r) and coercive field (E_C). At room temperature, P_S, P_r, and E_C are about 15.5 μC/cm^2, 14 μC/cm^2, and 2.2 kV/cm, respectively. This P_S from the R phase is considerably smaller than the 18–19 μC/cm^2 values seen in the 340–380 K range, which could be attributed to the T phase. Accordingly, at least part of the increase in P as the temperature increases to 355 K, as evidenced by the negative depolarization current density, could result from the polarization rotation of some regions from R via M_A to [001] T. The low permittivity above 355 K is consistent with T domains.

Both P_r and E_C reach a local maximum near 365 K and P_r exhibits a steep decline above $T_{re} = 410$ K. A "double hysteresis loop" was observed in the region of 400–420 K, as can be seen in Fig. 2(a), which is the characteristic of a P-E loop near a first-order transition. The double hysteresis loop indicates a discontinuous jump from a field-induced FE state to a paraelectric state at zero field. These phenomena are consistent with the re-entry of dielectric dispersion in $\varepsilon'_{PP\text{-}ZFH}$ and the positive depolarization current responses in Fig. 1(c). The polarization appears to retain some finite magnitude even above $T_m \cong 415$ K, as commonly seen in disordered materials, but this could result from a field-induced transition or from the finite measuring frequency of 46 Hz.

Figures 3(a) and 3(b) exhibit the room temperature ZFH domain structures with various micron-sized domains (less than 10 μm) randomly distributed in the matrix. Most of the matrix has an optical extinction at $P/A = 0°$ but a small fraction exhibits an extinction at $P/A \neq 0° \neq 45°$, indicating that a majority R phase mixes with M or rhombohedral nanotwin (R_{NT}) phases (which can mimic M_A and M_B phases).[24] The coexistence of the R and M or R_{NT} phases is confirmed by the (002) XRD, as shown in Fig. 4(a), which shows a strong R and a minor broad peak. The lattice parameter of the R phase was estimated to be $a = 4.025$ Å, which is fairly consistent with $a_R \cong 4.020$ Å that was obtained in Ref. 13 but is larger, perhaps because of the partly disorganized nature of this R phase in the ZFH crystal. Figure 5 shows the $\frac{1}{\sqrt{3}}$ ratio between the room temperature spontaneous polarizations $P_S \cong 15.5$ μC/cm^2 and $P_S \cong 27.0$ μC/cm^2, which were taken along [001] and [111], respectively, which confirms that R is the majority phase at room temperature. Note that $\frac{1}{\sqrt{3}}$ is the projection fraction of the [111] polarization on the [001] axis.

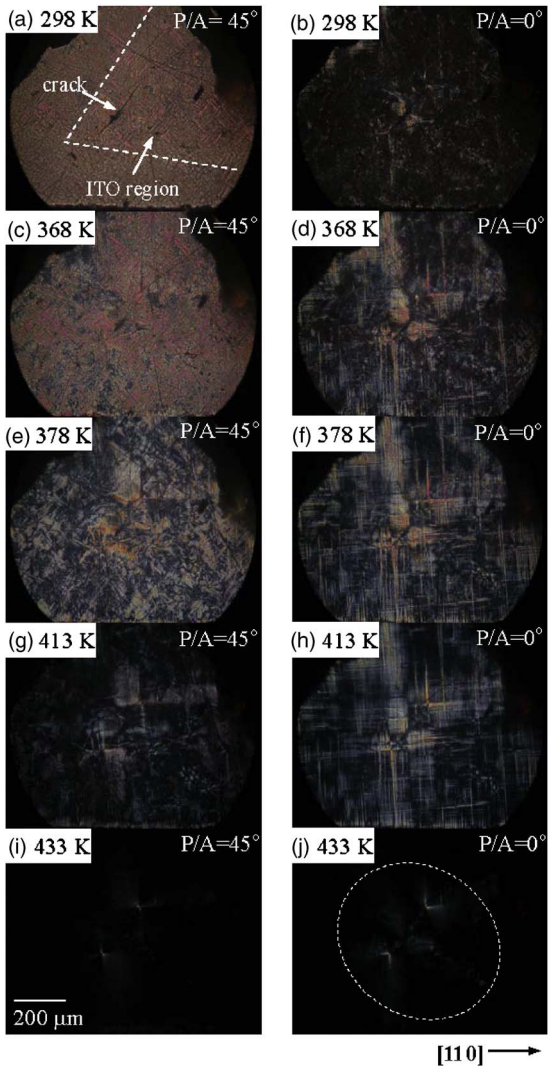

FIG. 3. (Color online) ZFH domain structures taken at $P/A = 0°$ and 45°. The dashed lines are the boundaries of the ITO films. The dashed circle indicates the region of incomplete total extinction.

As the temperature increases, as shown in Figs. 3(c) and 3(d), the domain matrix exhibits an obvious change in the region of 360–370 K. Besides some domains with an extinction angle at $P/A = 0°$, some domains rotate toward the T phase with extinction angles at $0 \leq P/A \leq 45°$, indicating M (or R_{NT}) and $T(T_{NT})$ phases. Note that tetragonal nanotwins (T_{NT}) can mimic the M_C phase with extinction angles at $P/A \neq 0°$.[23] $T(T_{NT})$ represents T nanotwins that mimic the M_C phase in the T matrix. The horizontal and vertical striations in Fig. 3(d) resemble those seen from the [100] and [010] T domains. This rotation toward the T phase is confirmed by the XRD in Fig. 4(c), in which the diffraction

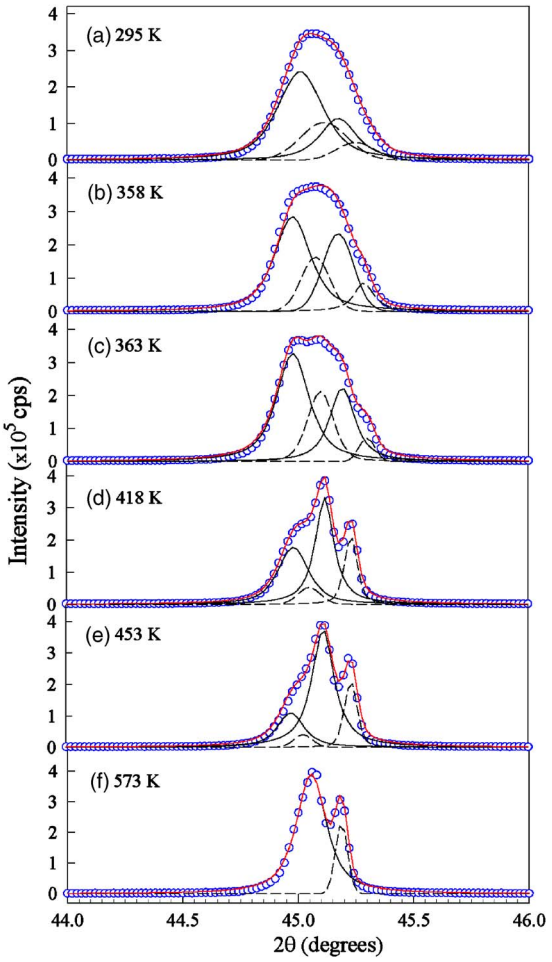

FIG. 4. (Color online) ZFH (002) XRD spectra. The solid and short-dashed lines correlate to the $K\alpha_1$ and $K\alpha_2$ radiations, respectively. The red solid line is the sum of the fitting curves.

shows an obvious change in contour and relative intensities and the right-hand peak becomes narrower and approaches the lattice parameter of the T phase found for PP-ZFH, as will be seen below. Note that the current density J_{ZFH} exhibits a small random response with up and down components in the region of 350–360 K. The inset in Fig. 1(a) shows a

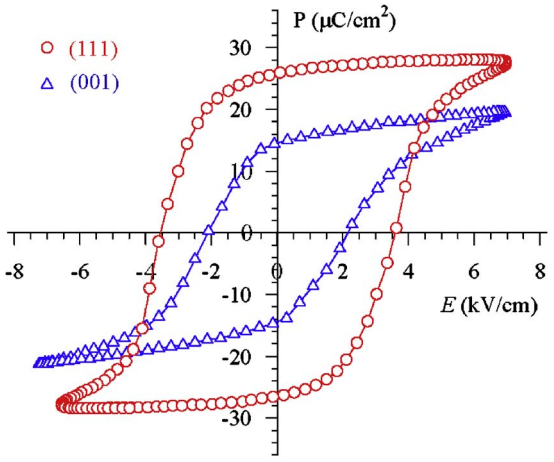

FIG. 5. (Color online) Hysteresis loops obtained from (001)- and (111)-cut crystals at room temperature.

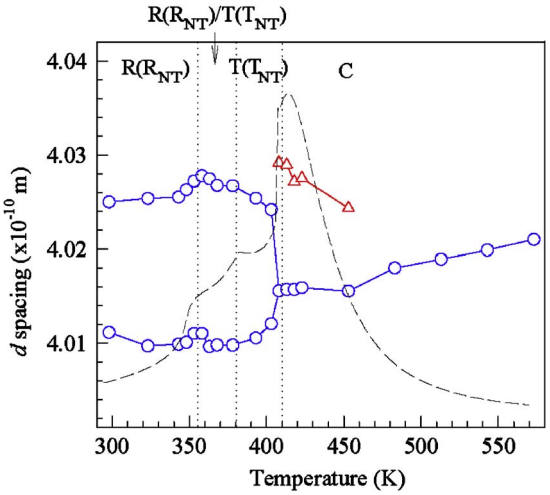

FIG. 6. (Color online) d spacing vs temperature for various phases in the ZFH process. The dashed line is ε'_{ZFH}. The dotted lines indicate the various transition temperatures. The triangle corresponds to the low-2θ lattice distortion.

thermal hysteresis near 355 K, indicating a first-order $R(R_{NT})$-$T(T_{NT})$ transition near 355 K, where ε'_{ZFH} exhibits a step-up anomaly upon heating. Near 378 K, as seen in Figs. 3(e) and 3(f), the domain matrix exhibits a significant evolution, in which the area with an extinction at $P/A=45°$ dramatically increases, indicating a major T phase, even though the striations seen at $P/A=0$ show little change. Note that ε'_{ZFH} exhibits a gradual step-up-like anomaly near 380 K in Fig. 1(a). However, there is no current response in J_{ZFH} [Fig. 1(a)] and the XRD shows only a gradual change in linewidth and lattice parameter, which corresponds to the appearance of the T phase. According to the eighth-order Devonshire theory analysis by Vanderbilt and Cohen,[29] both M_A-T and M_C-T transitions should be of second order, which may explain why no discontinuity appears in the current density and lattice parameter near 380 K, as seen in Figs. 1(a) and 6. Near 413 K, as seen in Figs. 3(g) and 3(h), the cubic (C) phase (with total extinction) begins to develop, which is associated with a partial T-phase matrix that does not show a total extinction.

As the temperature increases above $T_m \cong 415$ K, as seen in Figs. 3(i) and 3(j), the domain matrix does not immediately go into a complete total extinction (C phase), as indicated by the dotted circle in Fig. 3(j). Instead, in addition to the C phase, a low-2θ XRD shoulder, which remains up to about 450 K, was detected, as shown in Figs. 4(d) and 4(e). The broad shoulder is possibly due to lattice distortions caused by a local residual stress from the T-C transition or polar nanocluster material. The narrow C peak corresponds to the dipole glass material. Figure 6 gives the temperature-dependent d spacings in the ZFH process. In brief, the unpoled crystal proceeds by an $R(R_{NT})$-$R(R_{NT})$/$T(T_{NT})$-$T(T_{NT})$-C transition sequence near 355, 380, and 410 K.

The PP-ZFH domain structures after poling with $E=5$ kV/cm along [001] at room temperature are illustrated in Fig. 7. Percolating microdomains (green interference) were induced after poling with a size less than 30 μm and

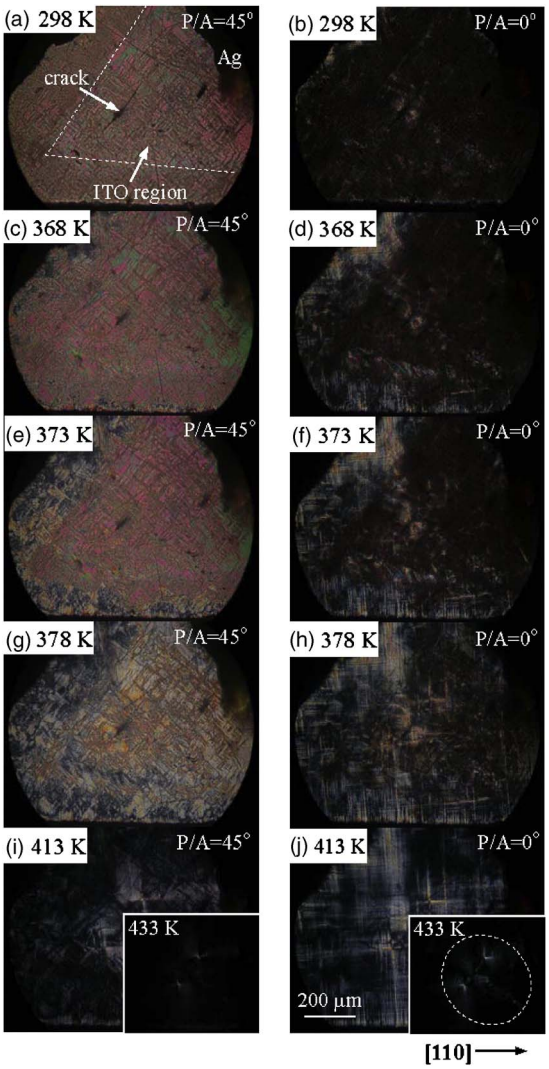

FIG. 7. (Color online) PP-ZFH (E=5 kV/cm) domain structures taken at P/A=45° and 0°.

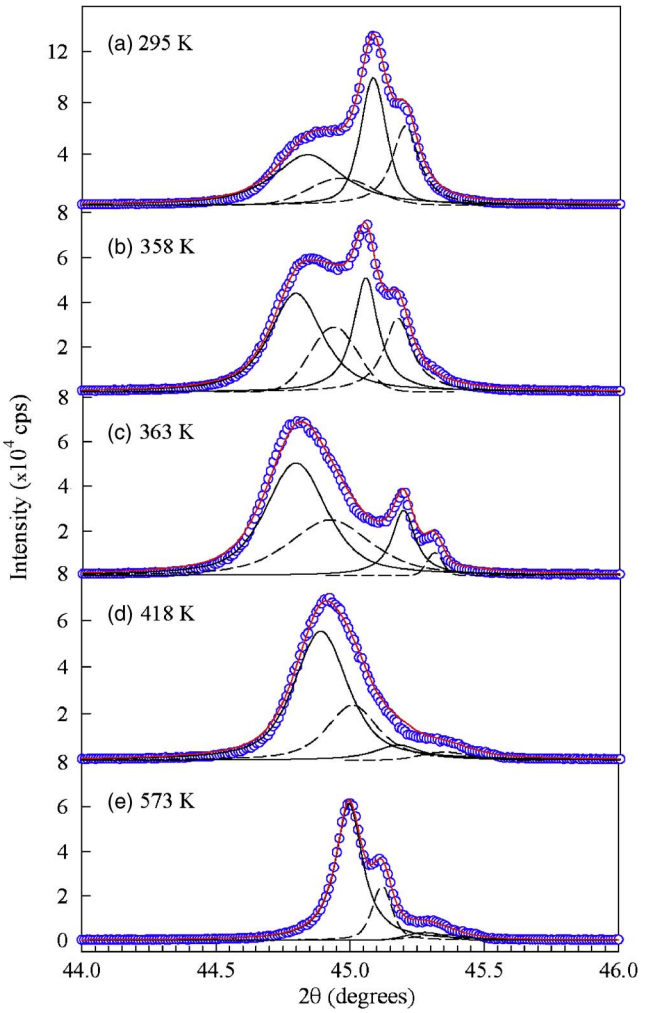

FIG. 8. (Color online) PP-ZFH (002) XRD spectra after poling at E =5 kV/cm. The solid and short-dashed lines correlate to the $K\alpha_1$ and $K\alpha_2$ radiations, respectively.

were randomly distributed in the matrix. The field-induced micrometric percolations were caused by rotating the polarizations of much smaller microdomains or nanoclusters into alignment so that the boundaries disappear. As shown in Figs. 7(a) and 7(b), most regions have an extinction angle at P/A=0°, indicating the coexistence of the R and R_{NT} phases. The coexistence of R and R_{NT} is confirmed by the (002) XRD in Fig. 8(a) with a sharper R peak and a broad peak. The broadening of the diffraction peak is due to coherent superimposition of scattered waves from individual nanodomains. Note that this R_{NT} assignment is to a peak to the left of the R peak, whereas in Figs. 4(a) and 4(b), the R_{NT} peak is to the right of the R peak. This only makes sense if the PP-ZFH R_{NT} (M_A and/or M_B) peak corresponds to the T_{001} peak because the prior poling prefers that orientation. From the 2θ fitting, the lattice parameter of the R phase was estimated to be a=4.019 Å.

As the temperature increases, some of the percolating microdomains (green) gradually grow with a maximum size of ~150 μm, as shown in Fig. 7(c). The extinction angle of most of the matrix stays at P/A=0° [Figs. 7(c)–7(h)]. However, the domain matrix exhibits no obvious change in the extinction angle near 355 K, where both the dielectric permittivity [Fig. 1(b)] and the polarization current [Fig. 1(c)] show a discontinuous first-order transition. It is important to note that tetragonal nanotwins (T_{NT}) can mimic an M_C phase with extinction angles close to P/A=0°. Note that the optimal resolution of the polarizing microscope is about 1 μm due to the optical diffraction limit. The low $\varepsilon'_{PP\text{-}ZFH}$ permittivity above 355 K in the [001] measuring field evidences a first-order $R(R_{NT})$-$T(T_{NT})$ transition. A rapid growth of the T_{NT} phase is verified near 360 K, as seen in Figs. 8(b) and 8(c), which shows a major broad T_{NT} peak (at low 2θ) with a T peak (at high 2θ). The d spacing also exhibits a discontinuous transition at 355 K, as shown in Fig. 9.

Near 378 K [Figs. 7(g) and 7(h)], the domain matrix radically turned to gray with extinction angles in the region of P/A=0–15°, which is likely associated with the breakdown of percolations and rapid development of polar tetragonal nanotwins (or polar tetragonal nanoclusters), as well as striations characteristic of T_{100} and T_{010} domains. The appearance of polar nanotwins can reduce the averaged optical birefringence and their dynamics causes a complete recovery of the dielectric relaxation near T_{re}=410 K.

The C phase (with total extinction) begins to develop

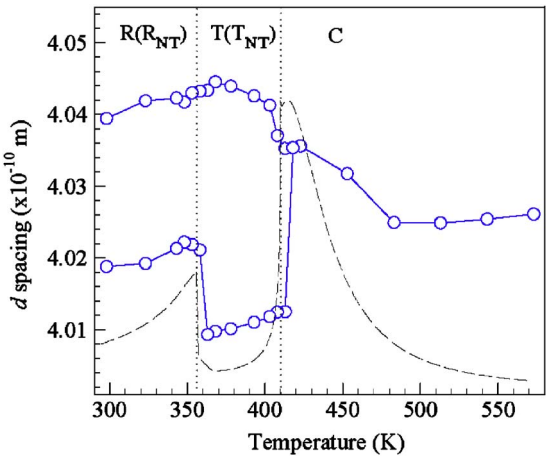

FIG. 9. (Color online) d spacing vs temperature for various phases. The dashed line is $\varepsilon'_{\text{PP-ZFH}}$. The dotted lines indicate the various transition temperatures.

near T_{re}=410 K, as shown in Figs. 7(i) and 7(j). This is consistent with the multiple-jump polarization current response in the region of 410–415 K [Fig. 1(c)] and the reappearance of the dielectric dispersion at T_{re}=410 K [Fig. 1(b)]. Above T_{re}=410 K, as indicated by the dotted circle in the inset of Fig. 7(j), the domain matrix does not immediately go into a complete total extinction (C phase). Instead, a high-2θ broad and weak shoulder was detected in the XRD, as shown in Figs. 8(d) and 8(e). This weak high-2θ broad peak is possibly attributed to lattice distortions caused by a local residual stress from the T-C transition or polar nanocluster material. In brief, the crystal is in a cubic state above T_{re}=410 K with polar nanoclusters, which immerse in the glassy matrix and vanish above T_B=510 K. Figure 9 is a summary of the $R(R_{NT})$-$T(T_{NT})$-C transition sequence taking place near 355 K and T_{re}=410 K in the PP-ZFH process.

The XRD data are perhaps the most difficult results to understand, and their discussion is interspersed above with the discussion of results from other techniques, so we present here a separate interpretation of the XRD data. In Figs. 4 and 8, for ZFH and PP-ZFH spectra, respectively, the narrow peaks come from well-organized larger regions of a given phase (R, T, or C), for which the $K\alpha_1$ and $K\alpha_2$ peaks are well resolved. Their separations obey the Bragg law $2\,d\sin\theta = n\lambda$. The broadening of the peaks is associated with nanotwins and is caused by the coherent superimposition of scattered diffraction waves.

Now, we consider the evolution of the XRD spectra with increasing temperature for both ZFH and PP-ZFH. At room temperature, the ZFH peak is broad, whereas the PP-ZFH spectrum has a narrow peak, which results from some well-organized R domains in addition to a broad peak from coherent diffractions of R nanotwins. As the temperature increases toward T_{re}=410 K, the ZFH peak gradually develops a structure, whereas the PP-ZFH spectrum exhibits a dramatic shift from a large narrow R peak at 355 K to a smaller but narrow $T_{100/010}$ peak at 363 K, while the broad peak strengthens from T nanotwins. The attribution of the sharp T peaks for both ZFH and PP-ZFH at 363 K is supported by both having the same d value of 4.009 Å.

Above T_{re}=410 K, both the permittivity and the polarizing microscopy results are similar for both ZFH and PP-ZFH, which indicates the gradual transformation of the remaining T-phase material to the C phase, so it may seem surprising that the XRD spectra for ZFH and PP-ZFH are quite different above 410 K. At 418 K, the ZFH intensity is divided into a sharp C peak with d=4.016 Å and a slightly weaker broad peak with d=4.027 Å. We attribute this broad peak to disorganized tetragonal nanotwins of average C symmetry because its d value is close to the value of d =4.035 Å for the single broad PP-ZFH peak at 418 K. The broad peaks can be attributed to the polar nanotwin (or nanocluster) material and the narrow peak to the dipole glass material. The ZFH broad peak becomes much weaker at 453 K and disappears before 573 K.

We can speculate that the less organized ZFH material below T_{re}=410 K contains considerable dipole glass material that easily transforms into a cubic dipole glass material at 410 K, giving the observed sharp C peak. By contrast, for PP-ZFH, the more ordered T material may transform at 410 K into mostly polar nanoclusters that then gradually transform into a cubic dipole glass and, finally, to an ordinary paraelectric C material above T_B.

Figure 10 shows the E-field-induced domain structures under $E \leq 38$ kV/cm along [001] at room temperature. At E=0 kV/cm, most parts of the domain matrix have an extinction angle of P/A=0°, indicating a majority R phase. As the E field increases [Figs. 10(c)–10(f)], more domains have extinctions at $P/A \neq 0°$, implying the expansion of the T_{NT} (or M_C) phase in the matrix. Under E=38 kV/cm [Figs. 10(g) and 10(h)], only a portion of the matrix became the [001] tetragonal phase, as indicated by "T_{001}," with an extinction at all P/A angles. The field-induced domain matrix exhibits irregular-shaped percolating microdomains that are randomly distributed in the matrix. This phenomenon implies that only part of the domain matrix can respond to an external E field. An internal crack (as indicated by the arrow) started to notably expand at $E \cong 10$ kV/cm along the [100] direction from the initial crack (initially caused by polishing). An irreversible E-field-induced effect was observed and the domain structures did not return to the original structures (before poling) after the E field was removed. Similar E-field-induced domain structures were observed in a (001)-cut PMN-24%PT crystal, in which percolating microdomains randomly embedded in the matrix and only part of the matrix turned into the T_{001} phase under E=44 kV/cm.[10]

IV. CONCLUSIONS

An $R(R_{NT})$-$R(R_{NT})/T(T_{NT})$-$T(T_{NT})$-C phase transformation sequence near 355, 380, and T_{re}(=410 K) was observed in a ZFH process. After a prior poling at E=5.0 kV/cm at room temperature, the crystal proceeds by an $R(R_{NT})$-$T(T_{NT})$-C transition sequence near 355 K and T_{re} =410 K upon heating. Rhombohedral nanotwins (R_{NT}) and tetragonal nanotwins (T_{NT}) play an important role in high-strain piezoelectric PMN-PT crystals while phase transitions take place because they can accommodate the spontaneous lattice distortion and minimize the elastic strain energy. It

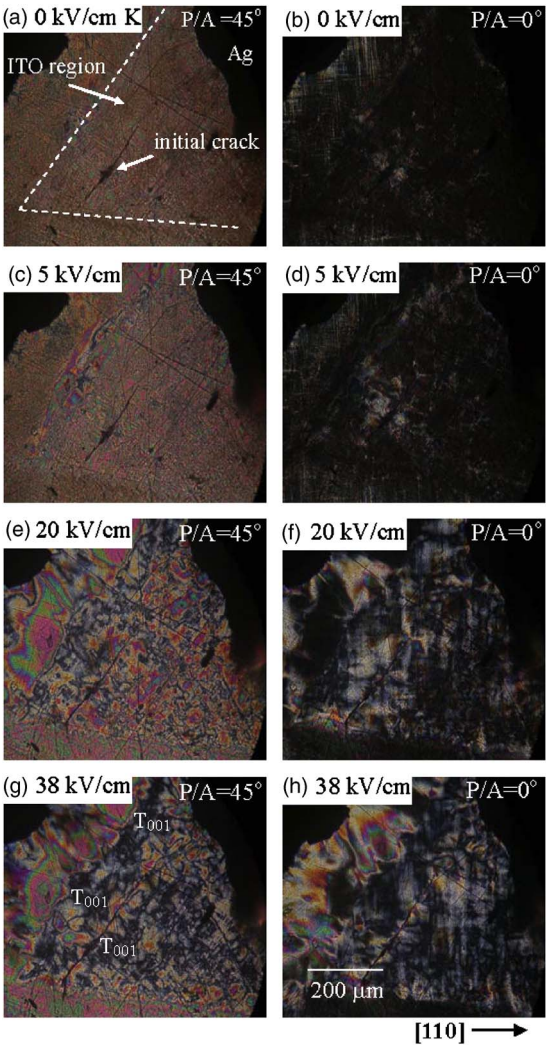

FIG. 10. (Color online) *E*-field-dependent domain structures obtained at $P/A=45°$ and $P/A=0°$.

was found that the R_{NT} and T_{NT} phases can be easily mistaken as monoclinic phases (M_A, M_B, or M_C). For example, an *R-M-T-C* phase sequence was proposed to exist in a (001)-cut PMN-30%PT crystal upon heating after the crystal was poled from the dielectric maximum temperature with $E=10$ kV/cm.[14] *E*-field-induced percolations were observed after a prior poling at $E=5$ kV/cm. A dramatic drop in permittivity occurs in the 355–410 K range and confirms an intrinsic $T(T_{NT})$ phase, whose nanotwins (or nanoclusters) play a key role in the re-establishment of the dielectric dispersion above 410 K. This work suggests that an intermediate *E*-field poling can induce microscopic percolations. Similar field-induced percolation and breakdown were seen in a (001)-cut rhombohedral PIN-30%PT crystal.[30]

The *E*-field-dependent domain study presents a partial confirmation of the ^{207}Pb NMR result, which proposes two components in the prototype PMN crystal, i.e., spherical glassy matrix and polar nanoclusters.[2] The FE nanoclusters are embedded in the glassy matrix and can be percolated into micrometric clusters by an external *E* field. The glassy matrix (probably the material in local random fields) less strongly responds to an *E* field than predicted by the Curie–Weiss law.

ACKNOWLEDGMENTS

The authors would like to thank Dr. H. Luo (Shanghai Institute of Ceramics) for the crystals. This work was supported by National Science Council of Taiwan Grant No. 96-2112-M-030-001.

[1] R. Blinc, V. V. Laguta, and B. Zalar, Phys. Rev. Lett. **91**, 247601 (2003).
[2] R. Blinc, V. V. Laguta, B. Zalar, and J. Banys, J. Mater. Sci. **41**, 27 (2006).
[3] R. Sommer, N. K. Yushin, and J. J. van der Klink, Phys. Rev. B **48**, 13230 (1993).
[4] I. K. Jeong, T. W. Darling, J. K. Lee, T. Proffen, R. H. Heffner, J. S. Park, K. S. Hong, W. Dmowski, and T. Egami, Phys. Rev. Lett. **94**, 147602 (2005).
[5] K. Hirota, Z.-G. Ye, S. Wakimoto, P. M. Gehring, and G. Shirane, Phys. Rev. B **65**, 104105 (2002).
[6] S. Tinte, B. P. Burton, E. Cockayne, and U. V. Waghmare, Phys. Rev. Lett. **97**, 137601 (2006).
[7] C.-S. Tu, R.R. Chien, F.-T. Wang, V.H. Schmidt, and P. Han, Phys. Rev. B **70**, 220103(R) (2004).
[8] Y. Yamashita, Y. Hosono, K. Harada, and N. Yasuda, IEEE Trans. Ultrason. Ferroelectr. Freq. Control **49**, 184 (2002).
[9] B. Noheda, D. E. Cox, G. Shirane, J. Gao, and Z.-G. Ye, Phys. Rev. B **66**, 054104 (2002).
[10] R. R. Chien, V. H. Schmidt, C.-S. Tu, L.-W. Hung, and H. Luo, Phys. Rev. B **69**, 172101 (2004).
[11] A. A. Bokov and Z.-G. Ye, J. Mater. Sci. **41**, 31 (2006).
[12] H. Fu and R. E. Cohen, Nature (London) **403**, 281 (2000).
[13] F. Bai, N. Wang, J. Li, D. Viehland, P. M. Gehring, G. Xu, and G. Shirane, J. Appl. Phys. **96**, 1620 (2004).
[14] Z. Feng, X. Zhao, and H. Luo, J. Appl. Phys. **100**, 024104 (2006).
[15] A. A. Bokov and Z.-G. Ye, J. Appl. Phys. **95**, 6347 (2004).
[16] Z.-G. Ye, B. Noheda, M. Dong, D. Cox, and G. Shirane, Phys. Rev. B **64**, 184114 (2001).
[17] G. Xu, H. Hiraka, G. Shirane, and K. Ohwada, Appl. Phys. Lett. **84**, 3975 (2004).
[18] G. Xu, Z. Zhong, Y. Bing, Z.-G. Ye, C. Stock, and G. Shirane, Phys. Rev. B **67**, 104102 (2003).
[19] P. M. Gehring, W. Chen, Z.-G. Ye, and G. Shirane, J. Phys.: Condens. Matter **16**, 7113 (2004).
[20] G. Xu, D. Viehland, J. F. Li, P. M. Gehring, and G. Shirane, Phys. Rev. B **68**, 212410 (2003).
[21] K. H. Conlon, H. Luo, D. Viehland, J. F. Li, T. Whan, J. H. Fox, C. Stock, and G. Shirane, Phys. Rev. B **70**, 172204 (2004).
[22] Z.-G. Ye, Y. Bing, J. Gao, A. A. Bokov, P. Stephens, B. Noheda, and G. Shirane, Phys. Rev. B **67**, 104104 (2003).
[23] Y. U. Wang, Phys. Rev. B **74**, 104109 (2006).
[24] Y. U. Wang, Phys. Rev. B **76**, 024108 (2007).
[25] H. Wang, J. Zhu, N. Lu, A. A. Bokov, Z. G. Ye, and X. W. Zhang, Appl. Phys. Lett. **89**, 042908 (2006).
[26] B. D. Cullity, *Elements of X-ray Diffraction*, 2nd ed. (Addison-Wesley, Reading, MA, 1978), pp. 8–10.
[27] S. Priya and K. Uchino, Jpn. J. Appl. Phys. **42**, 5158 (2003).
[28] D. Viehland, S. J. Jang, L. E. Cross, and M. Wuttig, Phys. Rev. B **46**, 8003 (1992).
[29] D. Vanderbilt and M. H. Cohen, Phys. Rev. B **63**, 094108 (2001).
[30] C.-S. Tu, R. R. Chien, C.-M. Hung, V. H. Schmidt, F.-T. Wang, and C.-T. Tseng, Phys. Rev. B **75**, 212101 (2007).